ARTICLE OPEN

Switchable valley splitting by external electric field effect in graphene/CrI$_3$ heterostructures

M. Umar Farooq[1] and Jisang Hong[1]

Achieving and controlling valley splitting is a core issue for valleytronics applications. Conventionally, valley splitting was achieved by applying an external magnetic field or structural manipulation. However, this approach is less efficient. Here, we explored single layer and bilayer graphene on CrI$_3$ (g-CrI$_3$ and 2g-CrI$_3$) heterostructures to induce valley splitting. In g-CrI$_3$, we found a valley splitting with the majority gap difference of $\Delta_{1\uparrow} - \Delta_{2\uparrow} = 44$ meV. Even in 2g-CrI$_3$ system, we also found valley splitting of $\Delta_{1\uparrow} - \Delta_{2\uparrow} = 21$ meV. Moreover, we also investigated the electric field effect on valley splitting. In both systems, we observed that valley splitting could be switched in the majority spin band. For instance, the sign of gap difference at $\pm$K changed from $\Delta_{1\uparrow} > \Delta_{2\uparrow}$ at zero field to $\Delta_{1\uparrow} < \Delta_{2\uparrow}$ at a small applied electric field of 0.1 V/Å. With further increase of the electric field to 0.2 V/Å, valley splitting disappeared. Thus, we propose that a large value of valley splitting can be achieved and the sign of splitting can also be switched with electric field instead of magnetic field. This feature may be beneficial for designing of valleytronic based information process devices.

INTRODUCTION

Valleytronics is now an emerging field in the condensed matter physics and extensive research efforts have been performed to utilize the valley index for device applications.[1–5] Indeed, the study on the valley physics started in the late 1970s using the two-dimensional (2D) electron gases in silicon inversion layers. In the beginning, the valley degeneracy and inter-valley coupling were investigated.[6–8] After the discovery of graphene, the interest in the valley physics began to grow substantially and the surge is ever-increasing with the help of advanced experimental technique to fabricate various types of 2D materials. Valley appears at corners of the hexagonal Brillouin zone (namely; ±K points) as degenerated states. Indeed, the valley index can behave as a distinguishable pseudospin in momentum space due to the opposite Berry curvature and extensive studies have been focused on the valley physics for potential device application by breaking the valley degeneracy.[3,4,9] In the graphene system, the pair of valley coincides with massless Dirac quasiparticles centered on these two inequivalent ±K corners of the Brillouin zone and this makes graphene a prime candidate for observing the physical properties associated with quantum Hall effects.[10]

Despite rich physics behind this phenomenon, the ability to control the valley pseudospin has a limitation due to the lack of intrinsic physical properties associated with valley occupancy.[11] The valley physics is closely related to the time reversal symmetry and we can differentiate the valley state by breaking the time reversal symmetry. It has been demonstrated that the valley splitting can be obtained by breaking the time reversal symmetry with an external magnetic field in monolayer MoSe$_2$.[12] However, it was required to apply a huge magnetic field to split the valley state and this is impractical for device applications. It was also proposed that the spin-valley coupling could induce intrinsic valley splitting.[13,14] On the other hand, it is possible to manipulate the valley state by making heterostructure with magnetic material. For instance, a large valley splitting in MoTe2/EuO(111) heterostructure was reported. Nonetheless, the metallic state appeared in MoTe$_2$ due to the interface effect and this characteristic may limit the device application.[15,16] As an alternative approach, it will be useful to use the 2D magnetic semiconductor material. Then, the valley manipulation can be possible by proximity effect.[17,18] Indeed, the control of valley splitting via flipping the CrI$_3$ magnetization through an external magnetic field is demonstrated in ultrathin ferromagnetic semiconductor CrI$_3$ and a monolayer WSe$_2$ heterostructure.[19] Recently, in graphene/BiFeO$_3$ heterostructures, a large spin splitting and the tuning of interfacial exchange coupling using the magnetic field were demonstrated.[20,21] The heterostructures can also be useful for achieving controllability of valley splitting by controlling the interlayer coupling, i.e., using perpendicular electric field. The manipulation of electric field is already performed in many experimental studies and easy to control it. Nonetheless, this potential valley control via gate voltage manipulation has not been yet explored. Here, we aim to study fundamental physical properties of graphene/CrI$_3$ heterostructure and propose that the tuning of valley degeneracy in graphene is possible by controlling the perpendicular gate voltage. In this report, we consider two types of heterostructures; a single graphene on CrI$_3$ and bilayer graphene on CrI$_3$. We find that a small external electric filed (~0.1 V/Å) can manipulate the magnitude of valley splitting and the sign of the gap in the majority spin band and the valley splitting is disappeared by further increasing the electric filed to 0.2 V/Å.

RESULTS AND DISCUSSION

Like a graphene, the pristine 2D CrI$_3$ has also a hexagonal structure and we performed structure optimization. The calculated

[1]Department of Physics, Pukyong National University, Busan 608-737, Korea
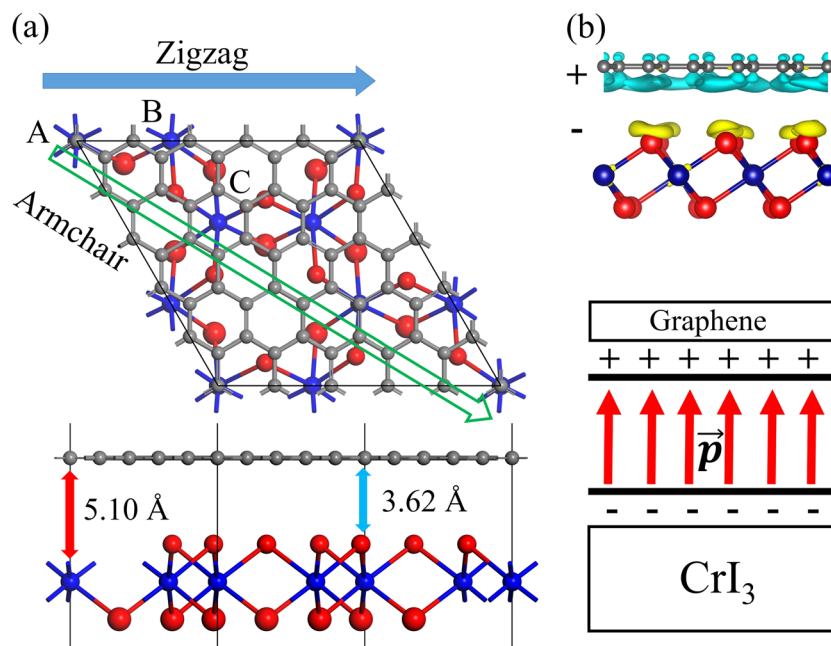Correspondence: Jisang Hong (hongj@pknu.ac.kr)

Fig. 1 **a** Top and side views of g-CrI$_3$ heterostructure. The blue, red and gray balls represent the Cr, I and C atoms. The red and blue arrows indicate the graphene to Cr and graphene to I interlayer distances. **b** charge density difference with the isosurface value of 0.00015 e/Å^3. The yellow and cyan represent the charge accumulation and depletion. Schematics illustration of dipole moment at the interface is shown at the bottom

lattice constant was 7.00 Å and this value is slightly larger than the experimental bulk value 6.867 Å.[22] Our calculation showed that the small change in the lattice constant did not have any significant effect on the electronic structure of CrI$_3$.[23] From the calculated lattice constant, we realized that the $\sqrt{3} \times \sqrt{3}$ CrI$_3$ supercell could be well matched with a 5×5 supercell of graphene with lattice mismatch around 1.7%. Figure 1a shows the crystal structure of a single layer graphene on CrI$_3$ (g-CrI$_3$). In this 2D heterostructure, several stacking geometries are possible depending on the lattice symmetries of the individual layer. However, in g-CrI$_3$ heterostructure, the peculiar atomic position mismatch of graphene and the CrI$_3$ layer rendered it impossible to find a specific staking structure with a conventional approach. Instead, many staking configurations are possible and it is rather complicated to find the most stable structure. To find the most stable configuration, we moved the CrI$_3$ layer along the zigzag and armchair directions with displacement interval of 0.1 Å until the equivalent of initial structure was obtained. We performed the atomic relaxation in each step. The calculated total energy difference was in the range energy from -100 to $30\,\mu eV$ per computational unit cell along the zigzag movement while it was about -50 to $50\,\mu eV$ along the armchair direction. We show the calculated results in Supplementary Information (SI) Fig. S1. This negligible energy difference indicates an almost frictionless movement. The calculated binding energy was 36.8 meV per unit carbon atom and this is comparable to the values found in other vdW systems. Despite the almost negligible total energy difference in different stacking configurations, the band structure can be different from each other. Thus, we calculated the band structures and found no substantial changes. The band structure after some displacement is presented in SI Fig. S2.

Due to the almost unchanged band structure and small energy difference in different configurations, we consider the configuration shown in Fig. 1a in the following discussion. As it is well-known, the pristine CrI$_3$ layer has a semiconducting band gap and the single layer graphene is a semi-metal with a zero gap. The

calculated work function of graphene is 4.21 eV and the electron affinity of CrI$_3$ is 4.64 eV. Consequently, the heterostructure has a typical metal-semiconductor contacted system. Nonetheless, there is no substantial charge transfer due to the vdW nature between two layers. Instead, a small charge redistribution in the space between two layers is possible. To check this, we calculated the charge density difference of a g-CrI$_3$ system given by

$$\Delta\rho(r) = \rho_{tot}(r) - \rho_g(r) - \rho_{CrI_3}(r) \tag{1}$$

where ρ_{tot}, ρ_g and ρ_{CrI_3} are charge densities of heterostructures (g-CrI$_3$), graphene and CrI$_3$. Figure 1b shows the calculated result. The yellow and cyan colors represent the charge accumulation and depletion. As shown, we observed charge redistribution at the interface and this resulted in an induced dipole moment of 0.203 e × Å. Figure 2a shows the band structure of g-CrI$_3$ without spin-orbit coupling (SOC). Compared with the band structure of the pristine CrI$_3$ layer, the dipolar field contributed to dragging down the CrI$_3$ band while the graphene band was elevated. Figure 2b shows the magnified band structure around the Dirac point. Note that the g-CrI$_3$ has a broken inversion symmetry and this symmetry breaking may create a band gap. However, we found almost linear dispersion at K-point in the minority spin band (spin down band) of the graphene layer. This indicates that the band gap opening due to symmetry breaking in minority spin band is negligible. In contrast, the majority spin band (spin up) of the graphene layer was hybridized with the CrI$_3$ majority band and the gap appeared. In graphene/WS$_2$ heterostructure, it was reported that the coupling of defect state between WS$_2$ and graphene bands near the Fermi level could cause large SOC effect in graphene and the spin Hall effect could occur even at room temperature.[24] Thus, we will also consider the SOC effect. It is worth of noting that the g-CrI$_3$ heterostructure does not have an inversion symmetry and time reversal symmetry due to the ferromagnetic CrI$_3$ layer. Consequently, we expect the degeneracy breaking of the band at the Dirac points ($\pm K$ points). Figure 2c shows the band structure after including the SOC. The Fig. 2d
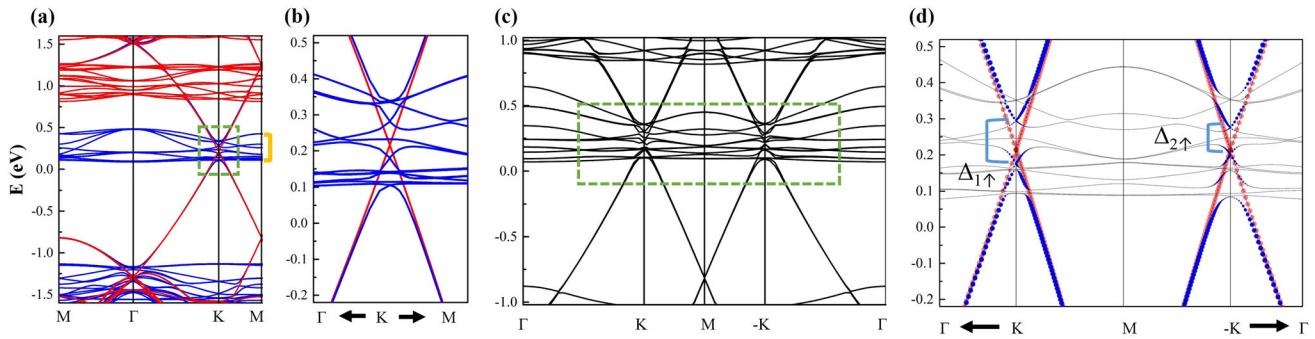
Fig. 2 Band structure of the g-CrI₃ with blue and red colors are representing the majority (spin up) and minority (spin down) states (**a**) without SOC (**b**) magnified band structure around the K point (**c**) band structure with SOC (**d**) magnified band structure with projections of graphene character near the ±K points
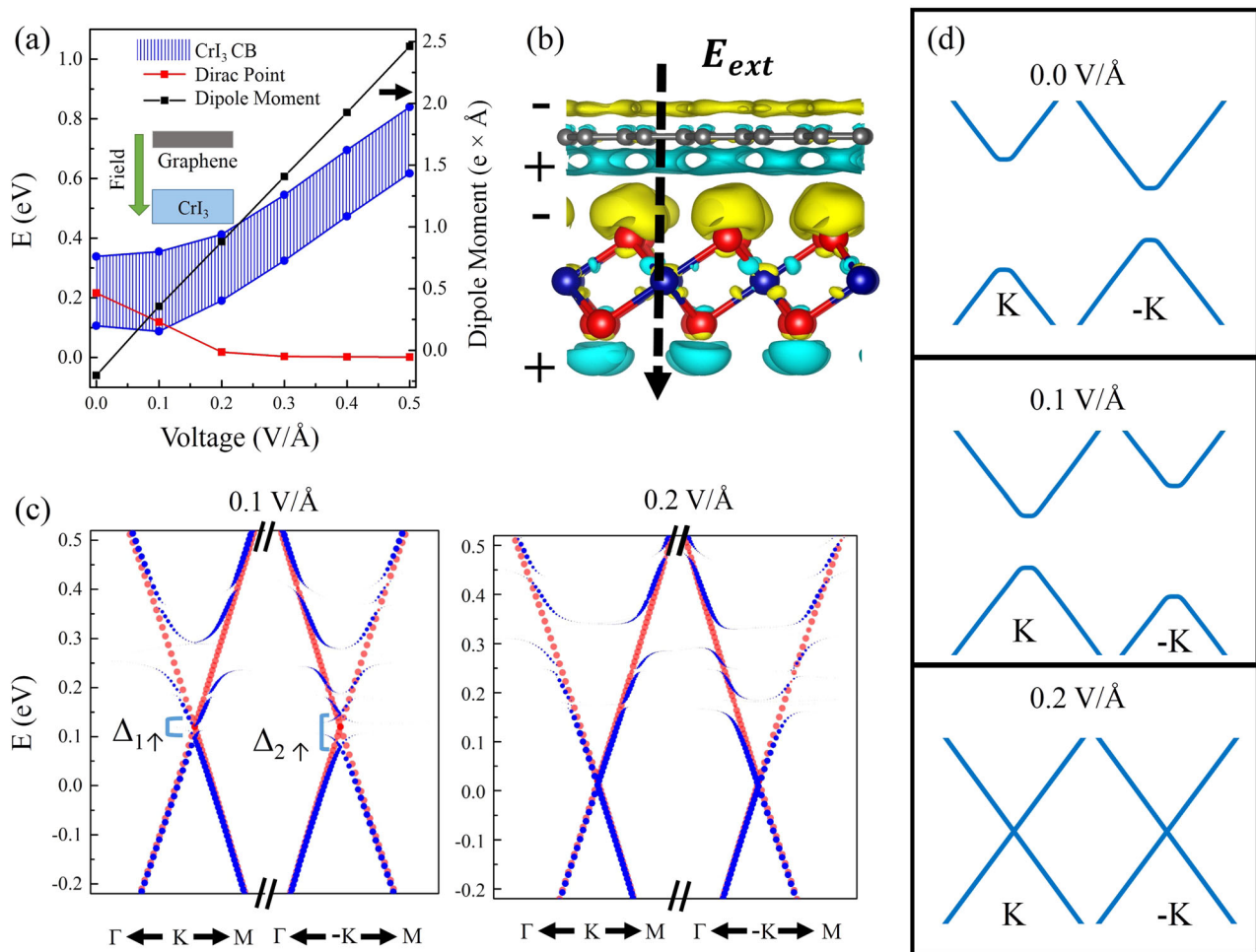

Fig. 3 Change in band structure of the g-CrI₃ under the applied field. **a** range of low-lying majority conduction band of CrI₃ majority spin state is represented by blue shaded area. Change of graphene Dirac point and dipole moment. The electric field direction is shown in the inset. **b** charge density difference at electric field of 0.2 V/Å. The isosurface value and colors are same as shown in Fig. 1b. **c** projections of graphene band around ±K with SOC under the electric field. **d** schematics illustration of sing change of valley splitting at ±K under the electric field

shows the magnified band with projections. Here, the blue and red colors represent the graphene majority (spin up) and minority (spin down) spin characters. The linear dispersion in the minority spin band of the graphene (red line) is still unchanged. However, the majority spin band character was affected due to the spin-dependent interaction. As shown, the majority spin bands of the

CrI₃ and the graphene were overlapped near the ±K points. Then, the majority electrons in the graphene experienced a periodic perturbative potential generated by the CrI₃ layer and this created the majority spin band splitting into a series of discrete pseudo-band in the energy range 0.1 ~ 0.4 eV above the Fermi level. If we define, the $\Delta_{1\uparrow}$ and $\Delta_{2\uparrow}$ as majority spin band gaps of graphene
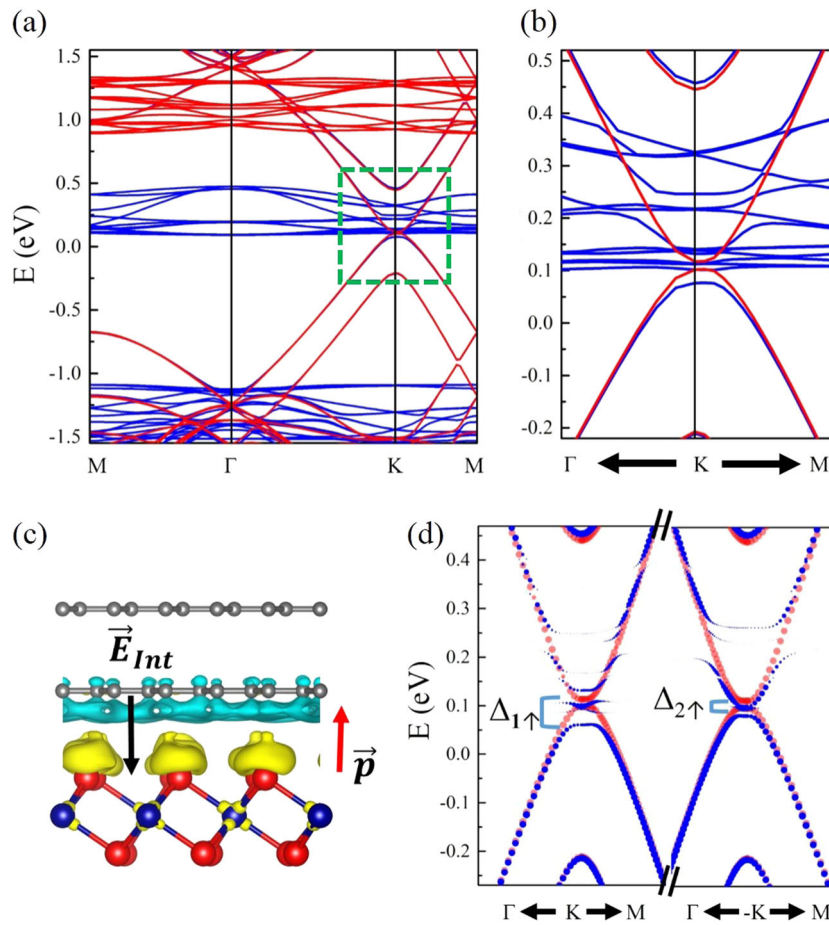
Fig. 4 **a** Band structure of the 2g-CrI$_3$ without SOC (**b**) magnified band structured around the K point (**c**) charge density difference with the same isosurface value and colors shown in Fig. 1b. (**d**) projected band of graphene around ±K points with SOC. The blue and red color in **a**, **d** represent the majority (spin up) and minority (spin down) states

layer at ±K-points, then the degeneracy breaking can be quantified from the gap difference $\Delta_{1\uparrow} - \Delta_{2\uparrow}$. The calculated values of $\Delta_{1\uparrow}$ and $\Delta_{2\uparrow}$ are 119 and 75 meV. This means that the pseudospin states at grapheme ±K valley are no longer degenerated and we obtain a huge splitting of $\Delta_{1\uparrow} - \Delta_{2\uparrow} =$ 44 meV in the majority spin states. This is due to the SOC effect in the absence of inversion and time reversal symmetry. Here, one should note that the CrI$_3$ band gap would strictly dependent on the choice of exchange and correlation functional. However, the previous theoretical study on g-CrI$_3$ system showed that the Dirac point location in conduction band of CrI$_3$ was insensitive to the functional.[23]

In the g-CrI$_3$ heterostructure, the Dirac point is located above the Fermi level and the energy level can be manipulated by applying the external electric field. Besides, the charge distribution will be altered under the influence of an external electric field and this will affect the electric dipole moment. Consequently, the overall band structure and valley splitting will be modified. Thus, we explored the effect of electric field effect on these issues. Figure 3a shows the change of the dipole moment (black line), the position of Dirac point (red line) for minority spin electron, and the energy interval of CrI$_3$ low-lying conduction band of majority spin (blue shaded region) at K-point when the electric field was applied from graphene to CrI$_3$. The band structure with the change of electric field is presented in the SI. Fig. S3. As discussed earlier, we observed a dipole moment from the CrI$_3$ to the graphene layer at

zero field. However, a sign change of the dipole moment with a small applied electric field appeared and this means that the direction of dipole moment is reversed. This can be understood from the charge redistribution owing to the electric field direction. As an illustration, we calculated the charge density difference by using the Eq. (1) at the electric field strength of 0.2 V/Å and Fig. 3b shows the calculated result. Besides, the Dirac point was shifted. With increasing the field strength, the Dirac point in the minority spin band lowered and located near the Fermi level while the low-lying majority spin conduction band of CrI$_3$ was completely separated from the Dirac point. Figure 3c shows the graphene band character around the ±K at the electric field of 0.1 eV/Å and 0.2 V/Å after the inclusion of SOC effect. At a small filed of 0.1 eV/ Å, the $\Delta_{1\uparrow}$ is 24 meV while the $\Delta_{2\uparrow}$ is 67 meV. Thus, we obtained the difference $(\Delta_{1\uparrow} - \Delta_{2\uparrow})$ of −43 meV. At 0.2 V/Å, the majority and minority spins at Dirac point almost coincided with the Fermi level at both ±K points and the valley splitting disappeared. Figure 3d shows the schematic of change in majority spin band at ±K under the electric field. At zero field, the valley degeneracy is broken with the $\Delta_{1\uparrow} > \Delta_{2\uparrow}$ while it was switched to $\Delta_{1\uparrow} < \Delta_{2\uparrow}$ at a small electric field of 0.1 V/Å. With further increase of the electric field, this degeneracy vanishes. This finding suggests that we can manipulate not only the valley degeneracy breaking but also the valley splitting sign change. We also investigated the physical properties by changing the direction of the applied electric field (CrI$_3$ to graphene direction). The calculated results are presented
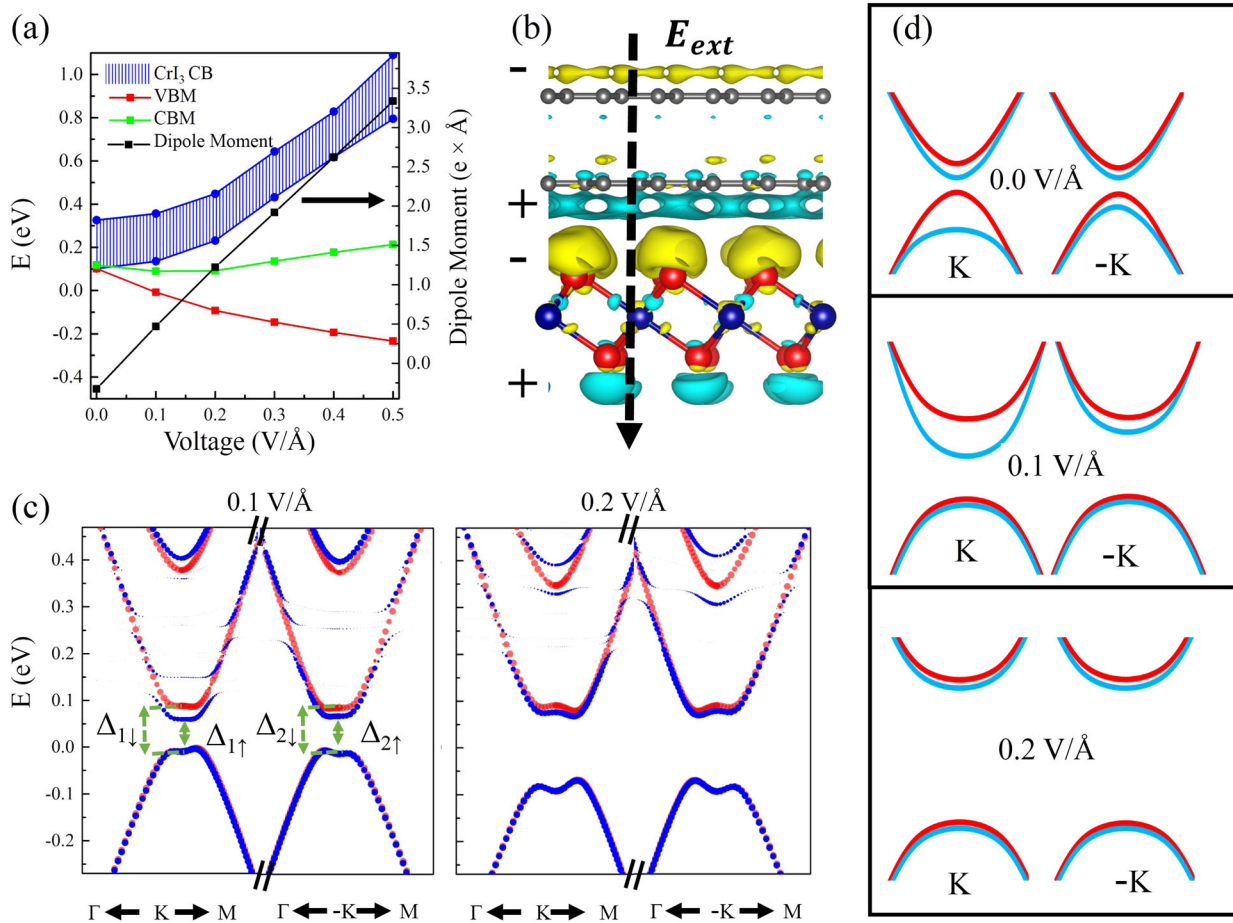
Fig. 5 Change in band structure of the 2g-CrI_3 under the applied field. **a** Range of low-lying majority conduction band of CrI_3 majority spin state is represented by blue shaded area. Change of CBM and VBM of graphene and change of dipole moment. **b** Charge density difference at electric field of 0.2 V/Å. The isosurface value and colors are same as shown in Fig. 1b. **c** Projections of graphene band around ±K with SOC under the electric field. **d** Schematics illustration of sing change of valley splitting at ±K under the electric field

in SI Fig. S4. In this case, the clear valley feature is blurred and consequently the valley degeneracy breaking is obscure.

We now discuss the bilayer graphene on CrI_3 (2g-CrI_3). Here, we consider AB type stacking in bilayer graphene. The intrinsic inversion symmetry of bilayer graphene can be broken by applying an external electric field and this will allow us to tune the band gap. Furthermore, we expect that the broken symmetry due to the field effect will be observed at two valleys (±K points). Figure 4a, b shows the band structure of 2g-CrI_3 without SOC at zero external electric field. In free standing bilayer graphene, it is well-known that the quadratic dispersion appears although the zero band gap is still preserved. In our 2g-CrI_3 heterostructure, we also find a quadratic dispersion at K-point. However, unlike the g-CrI_3, the bilayer 2g-CrI_3 had a band gap of 16 meV even in minority spin band. This band gap opening originates from the CrI_3 proximity effect. To understand this, we plot the charge density difference in Fig. 4c. In 2g-CrI_3 heterostructure, the charge inclination from graphene towards CrI_3 was enhanced compared with that in the g-CrI_3 system and we have a bit higher dipole moment ($\vec{p}$) of 0.325 e × Å. This means that we have a potential gradient across the bilayer graphene and this feature caused a band gap at Dirac point. In a recent experimental study, Shengwei et al. reported even a large band gap opening (~100 meV) of bilayer graphene sandwiched between antiferromagnetic bilayer CrI_3 and hexagonal boron nitride. This large gap can be the result of greater disorder in the graphene lattice under the experimental

condition.[25] Figure 4d shows the band structure with SOC effect. In the minority spin band of the graphene layer, the degeneracy at ±K was still preserved. However, in the majority spin band, we found the degeneracy breaking at the valleys (±K) and the energy difference $\Delta_{1\uparrow} - \Delta_{2\uparrow}$ was about 21 meV ($\Delta_{1\uparrow} = 37$, $\Delta_{2\uparrow} = 16$, $\Delta_{1\downarrow} = \Delta_{2\downarrow} = 16$ meV) although this value is smaller than that in g-CrI_3. We now discuss the electric field effect when the electric field is applied from the graphene to CrI_3 layer. Figure 5a shows the change of the dipole moment (black line), the change of conduction band minimum (CBM) state of graphene majority spin state, valence band maximum (VBM) of graphene majority spin state, and the energy interval of CrI_3 low-lying conduction band of majority spin electrons (blue shaded region) at K-point when the electric field was applied from graphene to CrI_3 layer. With increasing the electric field, the direction of electric dipole moment was changed and the low-lying conduction band of majority spin state in the CrI_3 layer was shifted upward. Besides, the band gap of the of graphene was further enhanced. Note that the band structures under the external electric field are presented in SI. Fig. S5. Figure 5b shows the charge density difference at the electric field strength of 0.2 V/Å. Like in the g-CrI_3, the application of electric field enforced the charge redistribution. This feature creates a big potential difference across the bilayer graphene and results in the enhancement of the graphene band gap. Figure 5c shows the projected band structure with SOC. We obtained band gaps of $\Delta_{1\uparrow} = 69.6$, $\Delta_{2\uparrow} = 81.2$, $\Delta_{1\downarrow} = 97.8$, and $\Delta_{2\downarrow} = 98.8$ meV for

each spin state at two valleys. Thus, the band gap difference $\Delta_{1\uparrow}$ $- \Delta_{2\uparrow}$ is about -12 meV for majority spin band while the gap difference $\Delta_{1\downarrow} - \Delta_{2\downarrow}$ is about 1 meV in the minority spin state. It was found that the valley splitting almost vanished with further increase of electric field. Figure 5d shows the schematic of change in the band at $\pm K$ under the electric field. Similar to the g-CrI$_3$ case, at zero field, the valley degeneracy is broken with the $\Delta_{1\uparrow} > \Delta_{2\uparrow}$ while it was switched to $\Delta_{1\uparrow} < \Delta_{2\uparrow}$ at a small electric field of 0.1 V/ Å. With further increase of the electric field, this degeneracy vanishes. This finding suggests that we can manipulate not only the valley degeneracy breaking but also the valley splitting sign change. We also investigated the physical properties when the direction of applied electric field was reversed (CrI$_3$ to graphene direction). The calculated results are presented in SI Fig. S6. In this case, the clear valley feature is blurred and consequently the valley degeneracy breaking is obscure.

We investigated the physical properties for the heterostructures of single and bilayer graphene on CrI$_3$ (g-CrI$_3$ and 2g-CrI$_3$). We found that the horizontal movement between planes was almost frictionless and the electronic band structure was also independent of stacking order. In g-CrI$_3$ system, due to the spin dependent coupling along with the absence of inversion and the time reversal symmetries, we obtained a large valley splitting with gap difference of 44 meV ($\Delta_{1\uparrow} - \Delta_{2\uparrow}$) at Dirac point ($\pm K$) in the majority spin states. In 2g-CrI$_3$ case, we also observed the valley splitting in the majority spin band although the gap difference at $\pm K$ points decreased to 21 meV ($\Delta_{1\uparrow} - \Delta_{2\uparrow}$). It was found that the valley splitting could be manipulated by an external electric field. In both g-CrI$_3$ and 2g-CrI$_3$, the sign of valley splitting was switched from $\Delta_{1\uparrow} > \Delta_{2\uparrow}$ at zero field to $\Delta_{1\uparrow} < \Delta_{2\uparrow}$ under a small electric field of 0.1 V/Å. This valley splitting was switched off with further increase of electric field to 0.2 V/Å. This finding indicates that the graphene valley pseudospin and the valley splitting manipulation is possible by controlling external the electric field. Since the use of electric field to control the physical properties is easy and efficient, our result may indicate that the graphene/CrI$_3$ heterostructure can be utilized for potential valleytronics applications.

METHODS

We performed all the calculations using the non-collinear density functional theory (DFT) with the application of Spin Orbit Coupling (SOC) as implemented in Vienna ab-initio simulation package (VASP).[26–28] Valence electrons were treated explicitly by plane wave method and their interactions with ionic cores were described by projected augmented plane wave pseudopotentials.[29,30] In our report, the generalized gradient approximation (GGA) was used for an exchange functional and correlation functional.[31] The plane-wave energy cut-off of 500 eV is used. The convergence criteria for energy is set to 0.001 meV. The DFT-D3 method of Grimme with Becke-Jonson damping is employed for van der Waals (vdW) corrections.[32] We imposed a vacuum region of 15 Å in the z direction for all calculations. All atomic positions relaxed until the residual forces on the atoms were smaller than 0.01 eV/Å.

DATA AVAILABILITY

The data related to the findings of this work is available from the corresponding author subject to reasonable request.

ACKNOWLEDGEMENTS

AUTHOR CONTRIBUTIONS

J.H. conceived the idea of this study and M.-U.F. performed DFT calculations. J.H. wrote the manuscript and M.-U.F. commented on it.

ADDITIONAL INFORMATION

Supplementary Information accompanies the paper on the npj 2D Materials and Applications website (https://doi.org/10.1038/s41699-019-0086-6).

Competing interests: The authors declare no competing interests.

Publisher's note: Springer Nature remains neutral with regard to jurisdictional claims in published maps and institutional affiliations.

REFERENCES

1. Bishop, N. C. et al. Valley polarization and susceptibility of composite fermions around a filling factor nu = 3/2. Phys. Rev. Lett. **98**, 266404 (2007).
2. Shkolnikov, Y. P., De Poortere, E. P., Tutuc, E. & Shayegan, M. Valley splitting of AlAs two-dimensional electrons in a perpendicular magnetic field. Phys. Rev. Lett. **89**, 226805 (2002).
3. Xiao, D., Yao, W. & Niu, Q. Valley-contrasting physics in graphene: magnetic moment and topological transport. Phys. Rev. Lett. **99**, 236809 (2007).
4. Yao, W., Xiao, D. & Niu, Q. Valley-dependent optoelectronics from inversion symmetry breaking. Phys. Rev. B **77**, 235406 (2008).
5. Rycerz, A., Tworzydło, J. & Beenakker, C. W. J. Valley filter and valley valve in graphene. Nat. Phys. **3**, 172–175 (2007).
6. Bloss, W. L., Sham, L. J. & Vinter, V. Interaction-induced transition at low densities in silicon inversion layer. Phys. Rev. Lett. **43**, 1529–1532 (1979).
7. Ohkawa, F. J. & Uemura, Y. Theory of valley splitting in an N-Channel (100) INversion Layer of Si III. Enhancement of splittings by many-body effects. J. Phys. Soc. Jpn. **43**, 925–932 (1977).
8. Sham, L. J., Allen, S. J., Kamgar, A. & Tsui, D. C. Valley-valley splitting in inversion layers on a high-index surface of silicon. Phys. Rev. Lett. **40**, 472–475 (1978).
9. Xiao, D., Chang, M.-C. & Niu, Q. Berry phase effects on electronic properties. Rev. Mod. Phys. **82**, 1959–2007 (2010).
10. Young, A. F. et al. Spin and valley quantum Hall ferromagnetism in graphene. Nat. Phys. **8**, 550–556 (2012).
11. Xu, X., Yao, W., Xiao, D. & Heinz, T. F. Spin and pseudospins in layered transition metal dichalcogenides. Nat. Phys. **10**, 343–350 (2014).
12. MacNeill, D. et al. Breaking of valley degeneracy by magnetic field in monolayer MoSe$_2$. Phys. Rev. Lett. **114**, 037401 (2015).
13. Li, X., Cao, T., Niu, Q., Shi, J. & Feng, J. Coupling the valley degree of freedom to antiferromagnetic order. Proc. Natl Acad. Sci. **110**, 3738–3742 (2013).
14. Liu, J. et al. Intrinsic valley polarization of magnetic VSe$_2$ monolayers. J. Phys. Condens. Matter **29**, 255501 (2017).
15. Qi, J., Li, X., Niu, Q. & Feng, J. Giant and tunable valley degeneracy splitting in MoTe$_2$. Phys. Rev. B **92**, 121403 (2015).
16. Zhang, Q., Yang, S. A., Mi, W., Cheng, Y. & Schwingenschlögl, U. Large spin-valley polarization in monolayer MoTe$_2$ on Top of EuO(111). Adv. Mater. **28**, 959–966 (2016).
17. Huang, B. et al. Layer-dependent ferromagnetism in a van der Waals crystal down to the monolayer limit. Nature **546**, 270–273 (2017).
18. Gong, C. et al. Discovery of intrinsic ferromagnetism in two-dimensional van der Waals crystals. Nature **546**, 265–269 (2017).
19. Zhong, D. et al. Van der Waals engineering of ferromagnetic semiconductor heterostructures for spin and valleytronics. Sci. Adv. **3**, e1603113 (2017).
20. Song, H.-D. et al. Asymmetric modulation on exchange field in a graphene/ BiFeO$_3$ heterostructure by external magnetic field. Nano. Lett. **18**, 2435–2441 (2018).
21. Wu, Y.-F. et al. Magnetic proximity effect in graphene coupled to a BiFe$_3$ nano- plate. Phys. Rev. B **95**, 195426 (2017).
22. McGuire, M. A., Dixit, H., Cooper, V. R. & Sales, B. C. Coupling of crystal structure and magnetism in the layered, ferromagnetic insulator CrI$_3$. Chem. Mater. **27**, 612–620 (2015).
23. Zhang, J. et al. Strong magnetization and Chern insulators in compressed graphene/CrI$_3$ van der Waals heterostructures. Phys. Rev. B **97**, 085401 (2018).
24. Avsar, A. et al. Spin–orbit proximity effect in graphene. Nat. Commun. **5**, 4875 (2014).
25. Jiang, S., Li, L., Wang, Z., Shan, J. & Mak, K. F. Spin transistor built on 2D van der Waals heterostructures. arXiv: 1807.04898 (2018).
26. Kresse, G. & Hafner, J. Ab initio molecular dynamics for liquid metals. Phys. Rev. B **47**, 558–561 (1993).

27. Kresse, G. & Hafner, J. Ab initio molecular-dynamics simulation of the liquid-meta -semiconductor transition in germanium. *Phys. Rev. B* **49**, 14251–14269 (1994).

28. Kresse, G. & Furthmüller, J. Efficient iterative schemes for ab initio total-energy calculations using a plane-wave basis set. *Phys. Rev. B* **54**, 11169–11186 (1996).

29. Blöchl, P. E. Projector augmented-wave method. *Phys. Rev. B* **50**, 17953–17979 (1994).

30. Kresse, G. & Joubert, D. From ultrasoft pseudopotentials to the projector augmented-wave method. *Phys. Rev. B* **59**, 1758–1775 (1999).

31. Perdew, J. P., Burke, K. & Ernzerhof, M. Generalized gradient approximation made simple. *Phys. Rev. Lett.* **77**, 3865–3868 (1996).

32. Grimme, S., Antony, J., Ehrlich, S. & Krieg, H. A consistent and accurate ab initio parametrization of density functional dispersion correction (DFT-D) for the 94 elements H-Pu. *J. Chem. Phys.* **132**, 154104 (2010).